Supplementary material to: Mantle earthquakes beneath Fogo volcano, Cape Verde: Evidence for subcrustal fracturing induced by magmatic injection

Carola Leva[1], Georg Rümpker[1], Frederik Link[1], Ingo Wölbern[1]

[1]Institute of Geosciences, Goethe-University Frankfurt, Altenhöferallee 1, 60438 Frankfurt am Main, Germany

1 - ARRAY LOCALIZATION METHOD

Arrays have the advantage that they are capable to localize earthquakes that are located outside a seismic network or events that lack sharp onsets. If the distance between the array and the event is significantly larger than the distance between the stations in the array an incoming wave can be treated as a plane wave (Schweitzer et al., 2012) that traverses the array with a certain backazimuth and an apparent velocity. The corresponding components of horizontal slowness (s_x,s_y), can be extracted by beamforming. For the array analysis we follow the procedure described in Singh and Rümpker (2018): First, a Buttherworth filter with cutoff frequencies determined from a spectral analysis is applied to enhance the seismograms under consideration. The first step of the array analysis is to choose a time window around the P-wave arrival with a length of about ten times of the dominant period (i.e. about one to two seconds in our case). Within this window a smaller stacking window is chosen of about one to two signal period length which is typically about 0.1 seconds. This is done with respect to the onset at the central array station which serves as a reference. The other traces are then shifted in time utilizing a grid

search scheme which accounts for all possible values of the horizontal slowness. In our examples, the grid search is performed within a slowness range of ±0.3 s/km.

Subsequently, the squared amplitudes of the traces (i.e. their energies) are stacked within the narrower stacking window. For a specific slowness (s_x,s_y), the beam energy reaches a maximum which represents the desired parameters of the event (i.e. absolute slowness and backazimuth). The inverse of the absolute slowness value yields the apparent velocity of the plane wave traversing the array. Uncertainties of backazimuth and slowness are estimated by considering resulting variations in slowness obtained from a 5% reduction of the maximum energy.

Our array on Fogo is designed for events with mean frequencies of 7.5 Hz, the stations are deployed on two rings around a central station with diameters of 700 and 350 m, respectively, see Figure S1.

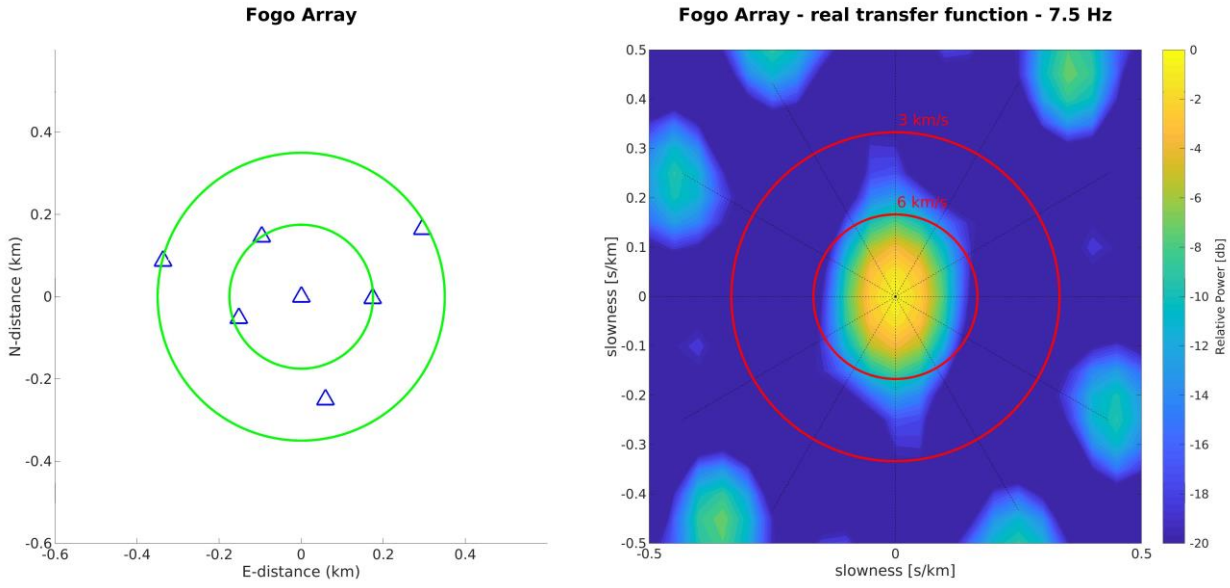

Figure S1: Left: array configuration, green circles: diameter of 700m and 350m, blue triangles: short period 4.5-Hz geophone stations. Right: resulting array transfer function for signals with a frequency of 7.5 Hz. Red circles: resulting apparent velocities of 3 km/s and 6 km/s, within which apparent velocities of incoming wavefronts are expected.

2 – VELOCITY MODELS

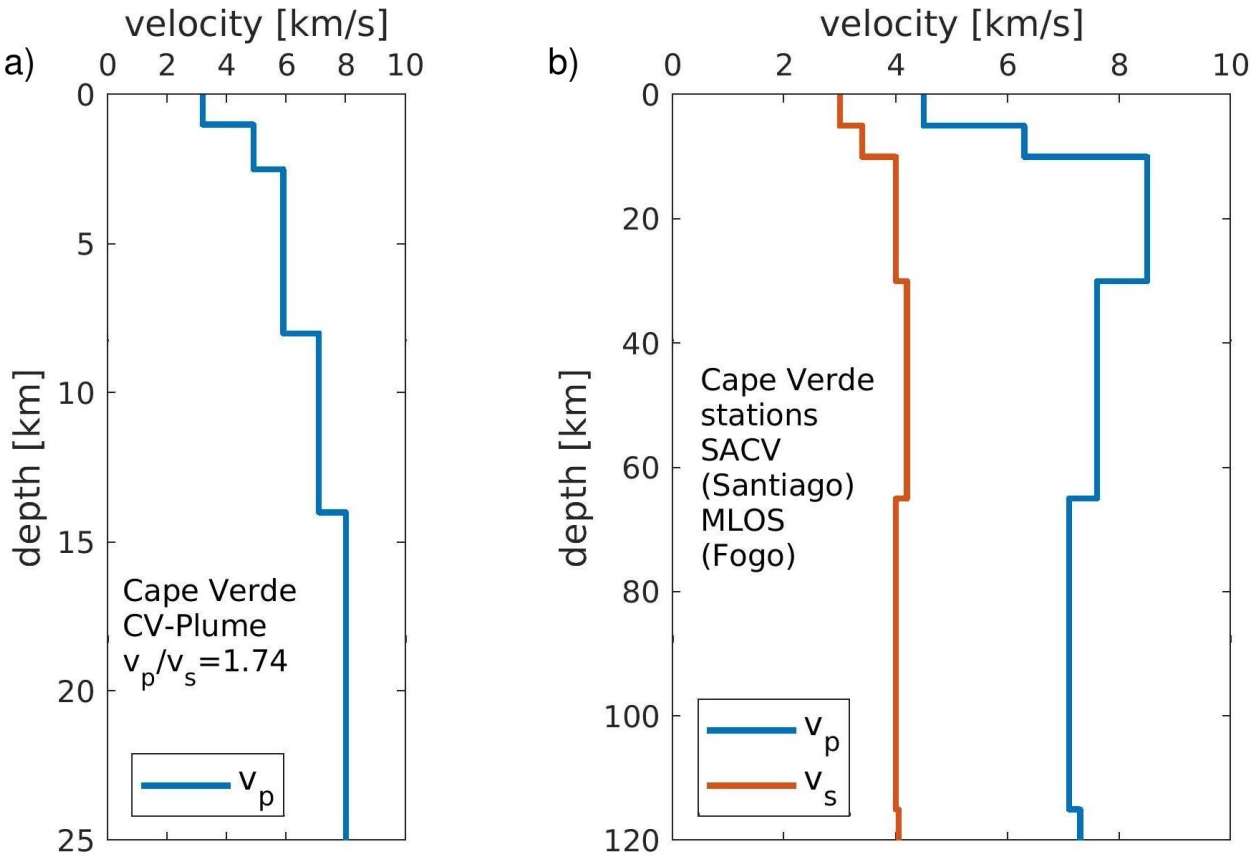

Figure S2: Velocity models for a) Cape Verde according to Vales et al. (2014), b) Santiago and Fogo (Cape Verde) adapted from Vinnik et al. (2012)

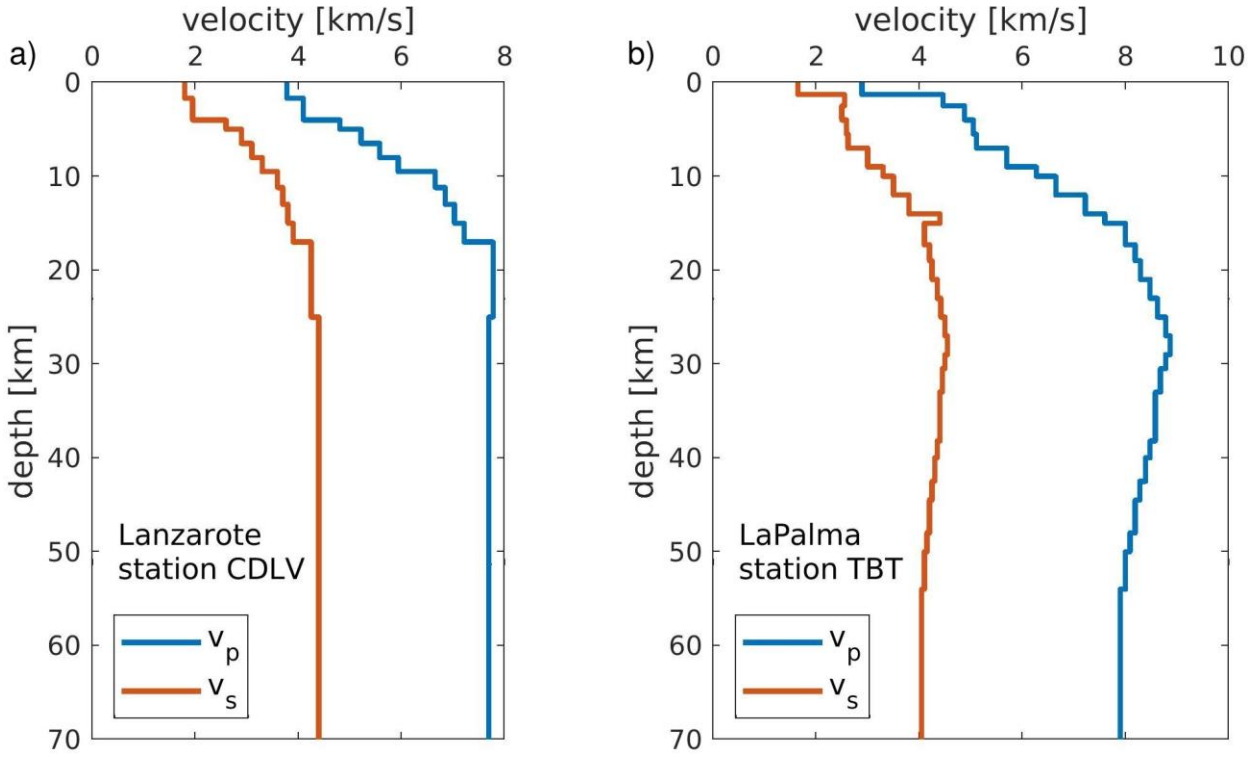

Figure S3: Velocity models for a) Lanzarote and b) La Palma (Canary Islands) adapted from Lodge et al. (2012)

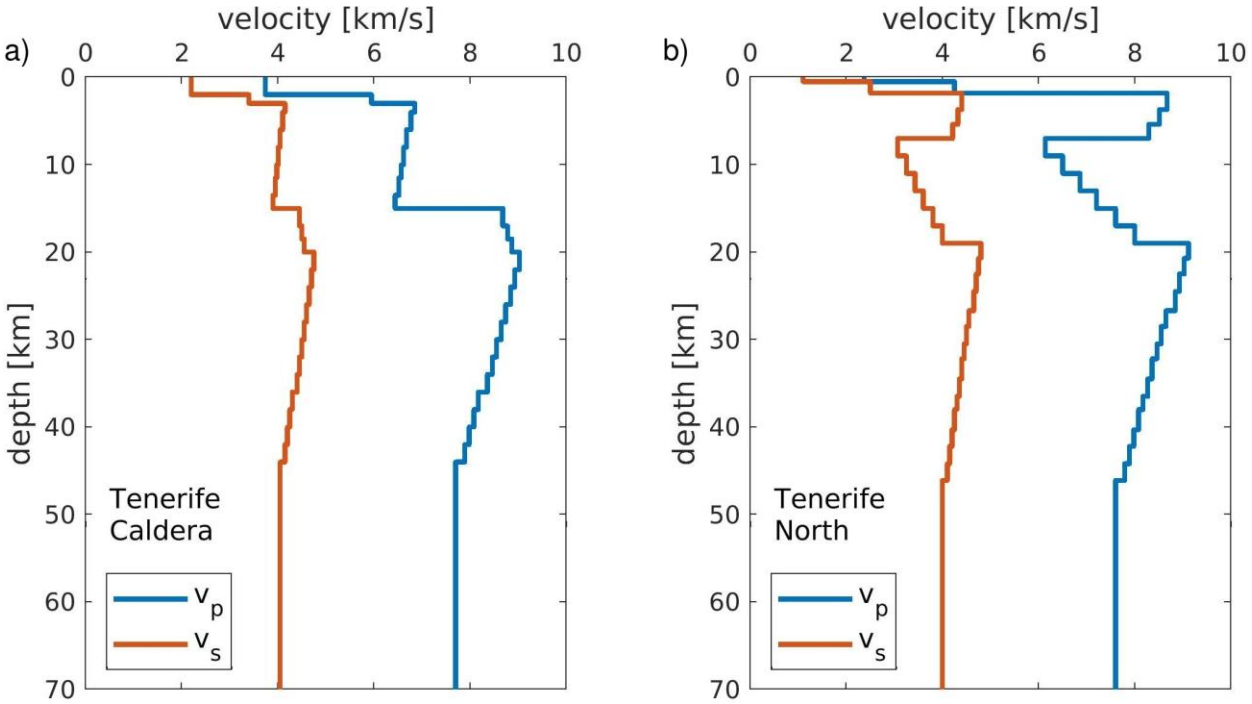

Figure S4: Velocity models for Tenerife (Canary Islands) a) derived from Caldera stations and b) northern stations, adapted from Lodge et al. (2012)

3 - TABLE OF RESULTS

TABLE S1: Results for the deep earthquakes of 15th August 2016

Time 15.08.2016 hh:mm.ss	Location		Location error		Depth (km)	Error depth (km)	STD error depth different vel. models (km)	Magni-tude	Usage of CV11*
	Lat (°)	Lon (°)	Lat (km)	Lon (km)					
05:05.54	14.903	-24.357	3.7	6.1	41.1	1.5	6.4796	1.2	No
05:12.20	14.910	-24.369	5.1	7.1	40.3	1.7	6.5625	0.9	No
05:33.36	14.873	-24.326	4.2	6.2	41.0	1.2	9.2414	0.8	No
05:36.23	14.852	-24.345	4.0	6.2	41.9	1.3	5.6656	0.9	No
05:50.43	14.948	-24.362	5.3	7.6	38.6	2.6	9.4967	0.8	No
05:51.41	14.904	-24.355	5.1	7.2	40.4	1.8	6.3502	0.8	No
06:01.17	14.897	-24.351	4.4	6.8	41.4	1.4	9.4299	1.2	No
08:48.05	14.834	-24.358	4.9	3.5	43.4	2.0	5.4453	1.6	Yes
09:59.42	14.876	-24.381	3.3	2.7	41.6	1.4	5.5301	2.1	Yes
11:57.39	14.880	-24.342	3.1	2.3	40.0	1.2	6.6500	1.4	Yes
13:27.15	14.826	-24.37	4.3	3.1	39.2	1.8	5.1760	1.4	Yes
14:36.50	14.837	-24.346	5.0	3.7	39.9	2.7	9.3357	1.5	Yes
15:57.09	14.889	-24.376	5.0	7.7	41.0	1.6	9.3170	1.3	No

Note: The error in depth is taken from the SEISAN code and does not include possible errors due to the velocity model. Different velocity models for some of the Canary Islands (Lanzarote, La Palma, Northern part of Tenerife, Caldera of Tenerife, taken from Lodge et al., 2012) are applied to derive the standard deviation (STD) of the depth estimate. These (larger) values are given as error bars in the figures.

*The last column indicates whether station CV11 was incorporated in the analysis.

4 – PARTICLE MOTION

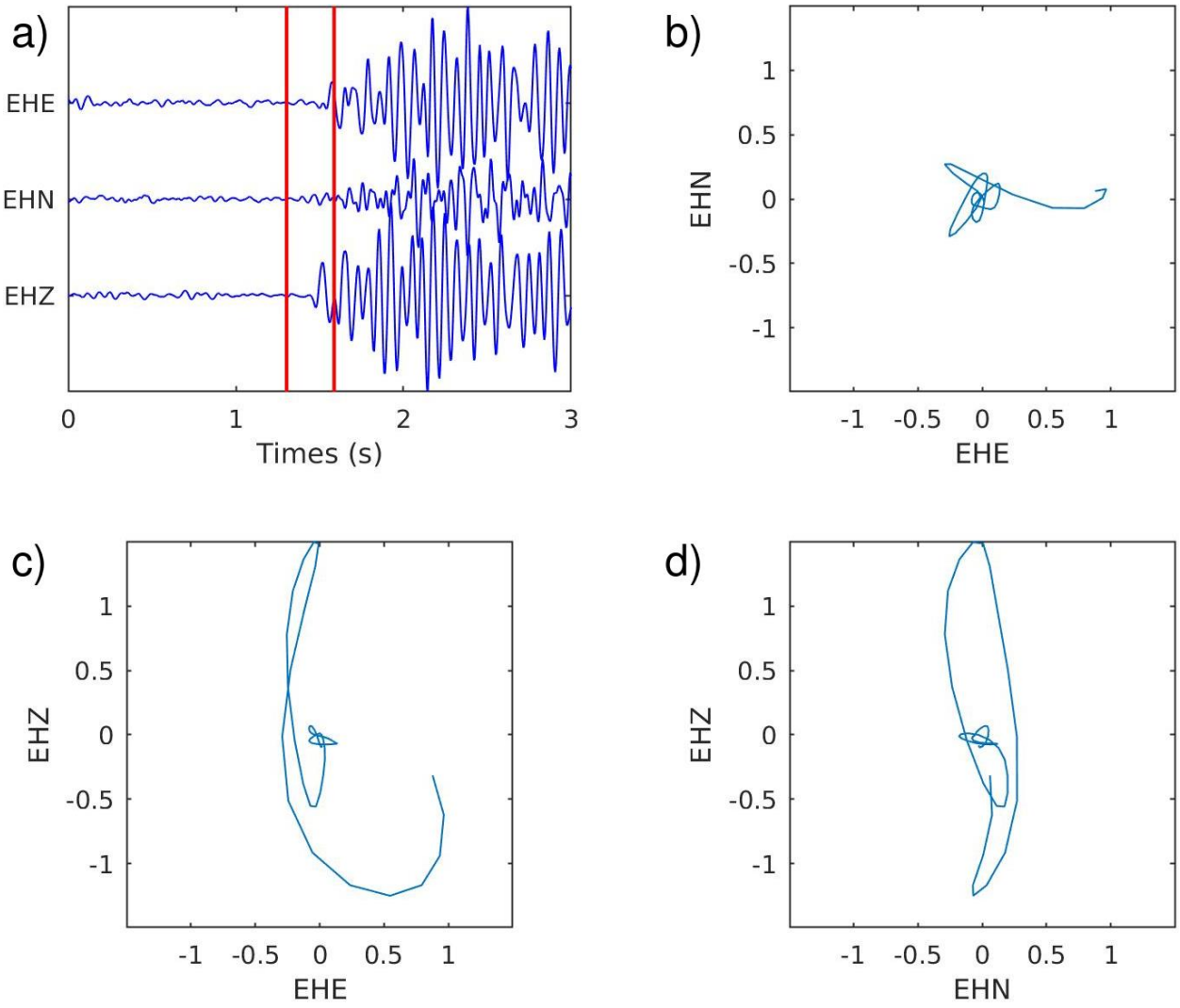

Figure S5: a) P-wave particle motion for the earthquake recorded on 15 August 2016 at 09:59 at a short-period station of the Fogo seismic array. The focal depth is 41.6 km. Traces are filtered between 1 and 16 Hz. The red lines indicate the time window used for the analysis. b)-d) Particle motion of the components EHN vs. EHE, EHZ vs. EHE and EHZ vs. EHN, respectively. The onset of the P-wave motion is clearly dominated by the vertical component EHZ.

5 – RECEIVER FUNCTION ANALYSIS

For the receiver function analysis to determine crustal thickness we follow the procedure of Zhu and Kanamori (2000). We introduced several quality criteria to obtain reliable receiver functions computed by a simple water level deconvolution (Langston, 1979).

Data quality and preparation

We use seismograms from teleseismic events recorded at our stations within epicentral distances between 35° to 95° and magnitudes above 5.5. Details on earthquake times, origin and recording stations are given in Table S2 and Figure S6, respectively. Receiver functions are calculated based on the deconvolution method described in Langston (1979).

The frequency analysis of pre-event noise and signal windows shows that the recordings are dominated by noise with frequencies down to 0.3 Hz. Therefore, data is filtered in bands of 0.05 to 0.3 Hz where the signal-to-noise ratio (SNR) is largest. The traces are rotated into the LQT-system using the theoretical backazimuth pointing into the direction of the epicenter and the incidence angle minimizing the energy on the radial component at time zero (after deconvolving the L-component from the Q-component) in a grid search. Finally, the P-receiver functions are computed by simple deconvolution in the frequency domain using a waterlevel of 0.005 to avoid instabilities (Langston, 1979).

Due to the short recording time, only few events are recorded at the individual stations. To further reduce the influence of noise we stack the energy grids for all stations assuming the same 1-D velocity model below all stations on Fogo. As the receiver functions are still relatively variable we use two additional quality criteria: First, we only use traces with a SNR of the Q-component of at least 1.2. Next, we discard traces, for which a significant Ps-phase cannot be

identified based on the sum trace of all receiver functions. From the 25 events, 28 receiver functions remain for the final analysis.

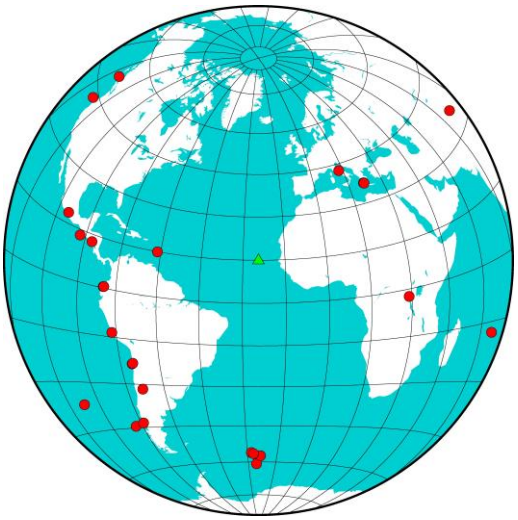

Figure S6: Distribution of the teleseismic earthquakes used in the receiver function analysis fulfilling all quality criteria (red circles). The green triangle marks the location of the seismic stations on Fogo.

Results of the receiver-function stacking

The left-hand side of Figure S7 shows the receiver functions sorted with respect to the slowness. The receiver functions exhibit a significant phase of positive amplitude at about 1-2 s which we interpret as a converted signal from the Moho discontinuity (see Figure S7). In contrast, the related multiples at later times are weak and scatter. This may be indicative of a transitional boundary between the crust and mantle in relation to magmatic underplating. Such a feature had been modeled and observed with receiver function data from Mauritius as reported by Singh et al. (2016). The right panel of Figure S7 shows the calculated energy grid which constrains the

values for the crustal thickness to 11.1 ± 4.5 km and the velocity ratio to 1.73 ± 0.12. To estimate the standard deviation of our results we applied a bootstrap analysis (Efron, 1979) by repeated application of the stacking procedure for different subsets of the receiver functions. Thirty percent of the traces are randomly discarded and replaced by copying a subset of the remaining traces (Efron, 1979).

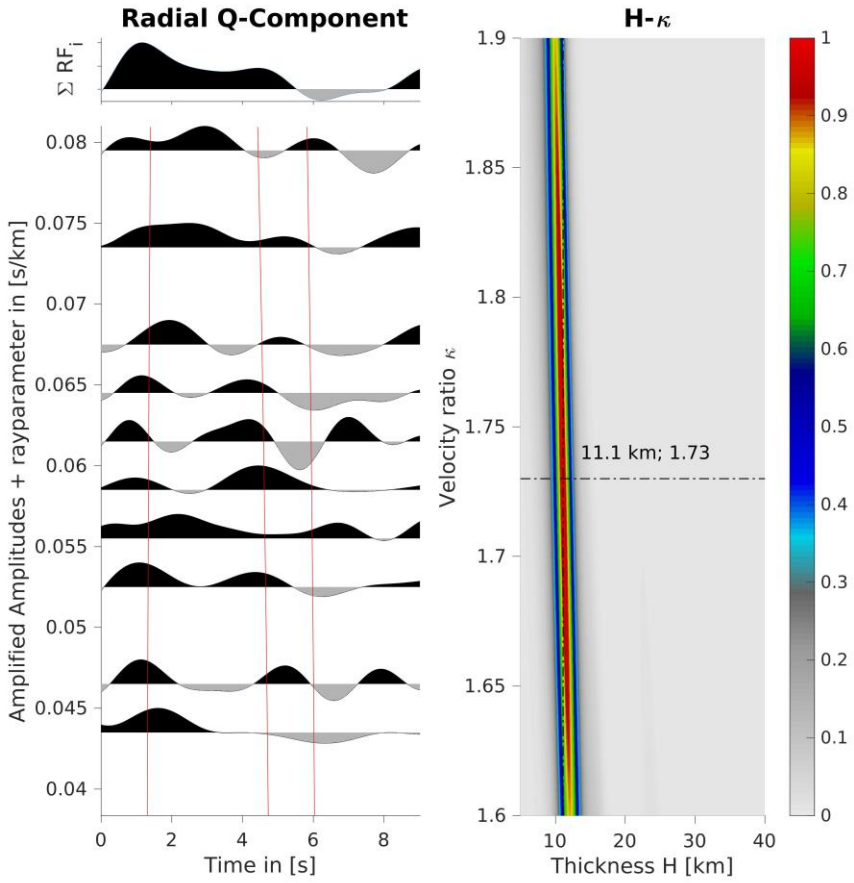

Figure S7: Receiver-function stacking to determine crustal thickness. Top left: Plain sum of the receiver functions. Bottom left: Stacked receiver functions sorted according to the ray parameter. The arrival times leading to the maximum of the stacking function are marked in red. Right: Stacking function for the crustal thickness and v_P/v_S ratio with maximum marked by dashed lines.

Table S2: Parameters of earthquakes used for receiver function analysis

Date	Time hh:mm:ss	Station	Lat (°)	Lon (°)	Magnitude	Distance (°)*
29 November 2007	03:26:22	CVFG1	-36.76	-97.4	6.3	85.65
29 November 2007	19:00:20	CVFG1	14.94	-61.27	7.4	35.52
29 November 2007	19:00:20	CVFG4	14.94	-61.27	7.4	35.71
29 November 2007	19:00:20	CVFG5	14.94	-61.27	7.4	35.6
7 December 2007	01:41:01	CVFG3	-13.52	-76.66	5.6	59.03
13 December 2007	05:20:21	CVFG5	-23.16	-70.48	6.0	58.84
16 December 2007	08:09:17	CVFG5	-22.95	-70.18	6.7	58.5
5 January 2008	10:39:14	CVFG1	51.32	-130.39	5.7	88.12
3 February 2008	07:34:12	CVFG1	-2.3	28.9	5.9	55.53
10 February 2008	12:22:02	CVFG1	-60.8	-25.59	6.6	75.44
14 February 2008	10:09:22	CVFG3	36.5	21.67	6.9	46.1
14 February 2008	12:08:55	CVFG1	36.34	21.86	6.5	46.41
14 February 2008	12:08:55	CVFG5	36.34	21.86	6.5	46.35
23 February 2008	15:57:20	CVFG5	-57.34	-23.43	6.8	71.96
20 March 2008	22:32:57	CVFG1	35.49	81.47	7.2	93.97
14 April 2008	09:45:19	CVFG5	-56.02	-28.04	6.0	70.7
28 April 2008	00:06:28	CVFG4	17.85	-100.17	5.8	72.39
20 May 2008	15:16:04	CVFG1	-44.45	-78.21	5.6	76.62
22 August 2008	07:47:39	CVFG2	-17.77	65.39	6.0	94.31
14 March 2016	07:26:40	CV10	-56.43	-27.01	5.6	71.12
15 April 2016	14:11:26	CV12	13.4	-92.37	6.1	65.6
18 May 2016	07:57:02	CV10	0.43	-79.79	6.7	56.61
18 May 2016	16:46:43	CV12	0.49	-79.62	6.9	56.3
10 June 2016	03:25:22	CV12	12.83	-86.96	6.1	60.52
24 August 2016	01:36:32	CV10	42.72	13.19	6.2	42.45
20 November 2016	20:57:44	CV10	-31.62	-68.63	6.4	62.81
28 November 2016	04:34:44	CV10	43.37	-127.02	5.5	88.82
25 December 2016	14:22:27	CV12	-43.41	-73.94	7.6	73.58

*Epicentral distances have been calculated using the software package TauP (Crotwell et al. 1999).

REFERENCES CITED IN THE SUPPLEMENTAL MATERIAL

Crotwell, H. P., Owens, T. J., and Ritsema, J., 1999, The TauP Toolkit: Flexible Seismic Travel-time and Ray-path Utilities: Seismological Research Letters, v. 70, p. 154–160, doi: 10.1785/gssrl.70.2.154.

Efron, B., 1979, Bootstrap Methods: Another Look at the Jackknife: The Annals of Statistics, v. 7, no. 1, p. 1-26, http://www.jstor.org/stable/2958830.

Langston, C.A., 1979, Structure under Mount Rainier, Washington, inferred from teleseismic body waves: Journal of Geophysical Research, v. 84, p. 4749-4762, doi: 10.1029/JB084iB09p04749.

Lodge, A., Nippress, S.E.J., Rietbrock, A., Gracía-Yeguas, A., and Ibáñez, J.M., 2012, Evidence for magmatic underplating and partial melt beneath the Canary Islands derived using teleseismic receiver functions: Physics of the Earth and Planetary Interiors, v. 212, p. 44-54, doi: 10.1016/j.pepi.2012.09.004.

Schweitzer, J., Fyen, J., Mykkeltveit, S., Gibbons, S.J., Pirli, M., Kühn, D., Kværna, T., 2012, Seismic Arrays: Bormann, P. (Ed.), New Manual of Seismological Observatory Practice 2 (NMSOP-2), Potsdam: Deutsches GeoForschungsZentrum GFZ, p. 1-80, doi: 10.2312/GFZ.NMSOP-2_ch9.

Singh, M., Kaviani, A., and Rümpker, G., 2016, The crustal structure beneath Mauritius from teleseismic P receiver functions: Oceanic or continental?: Geophysical Research Letters, v. 43, p. 9636–9643, doi:10.1002/2016GL070529.

Singh, M., and Rümpker, G., Intraplate seismicity around Rodrigues Ridge (Indian Ocean) from time-domain array analysis: submitted to Journal of Geophysical Research: Solid Earth, 2018, (under revision)

Vales, D., Dias, N.A., Rio, I., Matias, L., Silveira, G., Madeira, J., Weber, M., Carrilho, F., and Haberland, C., 2014, Intraplate seismicity across the Cape Verde swell: A contribution from a temporary seismic network: Tectonophysics, v. 636, p. 325-337, doi: 10.1016/j.tecto.2014.09.014.

Vinnik, L., Silveira, G., Kiselev, S., Farra, V., Weber, M. and Stutzmann, E., 2012, Cape Verde hotspot from the upper crust to the top of the lower mantle: Earth and Planetary Science Letters, v. 319-320, p. 259-268, doi: 10.1016/j.epsl.2011.12.017.

Zhu, L., and Kanamori, H., 2000, Moho depth variation in southern California from teleseismic receiver functions: Journal of Geophysical Research, v. 105, p. 2969–2980, doi: 10.1029/1999JB900322.